Journal of Sound and Vibration (2001) **247**(5), 857–874
doi:10.1006/jsvi.2001.3754, available online at http://www.idealibrary.com on IDEAL®

VERTICAL VIBRATION ATTENUATION IN RAILWAY TRACK: A WAVE APPROACH

R. HILDEBRAND

MWL, Department of Vehicle Engineering, KTH (Royal Inst. of Technology), SE-100 44 Stockholm, Sweden. E-mail: robert@fkt.kth.se

(*Received* 22 *February* 2000, *and in final form* 18 *April* 2001)

A wave approach is used to determine the attenuation of vertical bending vibrations along an infinite railway track. An innovation is the inclusion of the effects of the second rail, and particularly the "mode" defined by its phase delay with respect to the vibrations of the first rail. This "mode" could refer to the two rails vibrating symmetrically (in-phase) or antisymmetrically (out-of-phase), for example. The results show that this "mode" shape can strongly influence the attenuation at some frequencies. A small parametric study provides results on the effect of some track design parameters on the attenuation behaviour.

1. INTRODUCTION

The track is the main source of radiated noise below about 1250 Hz, and a significant source up to 2000 Hz [1], from train pass-byes at all but the highest speeds (about 300 km/h [2]). Consequently, some considerable effort has been made in the predictive modelling of rail vibrations.

Vibration is *excited* in a rail because of some process involving interaction with the railway wheels; the process could be rolling with surface roughness, wheel impact against a rail joint, etc. Once in the rail, it *propagates* away from the wheel area, as "structure-borne sound", which decays with distance (from the source area), mainly by entering into the sleepers and ballast where the losses are high. Finally, the vibrating track *radiates* airborne sound to the wayside, to an extent which depends on the attenuation (spatial decay rate) in the track [3]. The focus here is on the second of these three steps: propagation, and more specifically on the in-track attenuation.

To further delimit the subject area, attention is (mostly) restricted to the far field region of the vibration source. The bending near field of the wheel contact point, a zone of initially rapid decay away from the source, is discussed very little. In the far field, the attenuation may be described by an "attenuation constant" a, which is the exponential decay rate with distance along the track. Additionally, the analysis is restricted to vertical bending vibrations.

Indeed, models already exist to describe vibrations in railway track, including both advanced time-domain models, such as references [4, 5], as well as frequency-domain models such as in references [6–13]. The innovation provided here, in light of these existing models, is the use of an efficient transfer matrix approach in the frequency domain for a track with discrete, flexible sleepers, and taking account of the second rail, which is shown to be of some significance. Reference [6] has flexible sleepers, and coupling of the two rails,

0022-460X/01/450857 + 18 $35.00/0

but the rail is continuously supported. Reference [7] has discrete, flexible sleepers, but does not take the second rail into account. The other frequency-domain models listed had lumped element models for the sleepers, discrete in some cases, and did not couple the two rails. The significance of the beam-like character of the sleepers is well demonstrated in reference [7] by the appearance of low-attenuation bands at frequencies corresponding to sleeper modes, and in reference [6] by maxima of sleeper displacements and strains at these frequencies.

2. METHOD

The model is formulated by regarding, in sequence, (1) the geometric and physical description of the track, (2) the waves and decaying near fields into and out of a "junction" (intersection between a rail and a sleeper) in all directions, (3) the physical conditions of continuity and connectedness at the junctions, (4) conditions connecting the junction to the rest of the track and (5) methodology for obtaining the attenuation.

2.1. GEOMETRY AND PHYSICAL DESCRIPTION

The physical model of the track, and the co-ordinate system, is given in Figure 1. The rail and sleeper are modelled as Timoshenko beams, with hysteresis losses provided by complex bending stiffnesses. The pad is a lumped stiffness with hysteretic damping (complex stiffness). The ballast is a locally reacting Winkler foundation with *viscous* losses. The

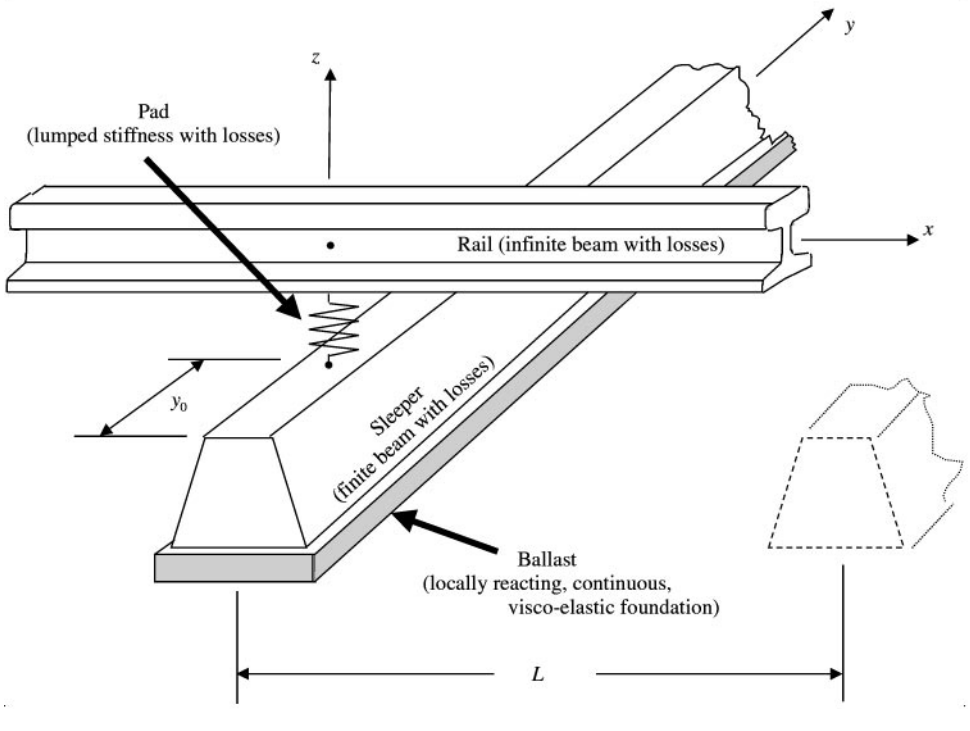

Figure 1. Physical model and co-ordinate system.

symbols for physical parameters of the track, as well as reference values used in calculations, are given in Appendix B (for a typical Swedish light track with UIC-50 rails).

One can conceive of refinements to this physical model, such as, for example, rotational pad stiffnesses, varying sleeper cross-section, or alternative damping models. Using a reasonable ratio of rotational-to-translational pad stiffness, however, and the frequency range considered in this paper, a quick calculation shows that the power supplied to the rail by the moment reaction at a pad is at least an order of magnitude less than that supplied by the force reaction. It seems therefore justified, in a simple model, to ignore the rotational pad stiffness. Similarly, the bending stiffness of a typical Swedish concrete sleeper varies by at most about 25% along its length, giving only about 6% variation in the (Bernoulli) bending wavenumber. Wooden sleepers vary even less along their length. The combination of damping models selected (viscous for the ballast, hysteretic elsewhere) was found in reference [7] to give the best results.

2.2. WAVES

Attention is given to a junction. Four regions ("approaches") are defined (see Figure 2): *A* rail, left of the junction; *B* rail, right of the junction; *C* sleeper, inside the rails and *D* sleeper, outside of the rails.

At each approach point (*A*, *B*, *C*, *D*), the displacement z consists of four terms: two oscillating ($e^{\pm ikx}$-type) and two decaying ($e^{\pm kx}$-type). This gives a total of 16 complex amplitudes per junction, the elements of **w**:

$$z_A = (w_3 e^{ik_{rB}x} + w_4 e^{k_{rN}x} + w_{11} e^{-ik_{rB}x} + w_{12} e^{-k_{rN}x}) e^{i\omega t}, \tag{1}$$

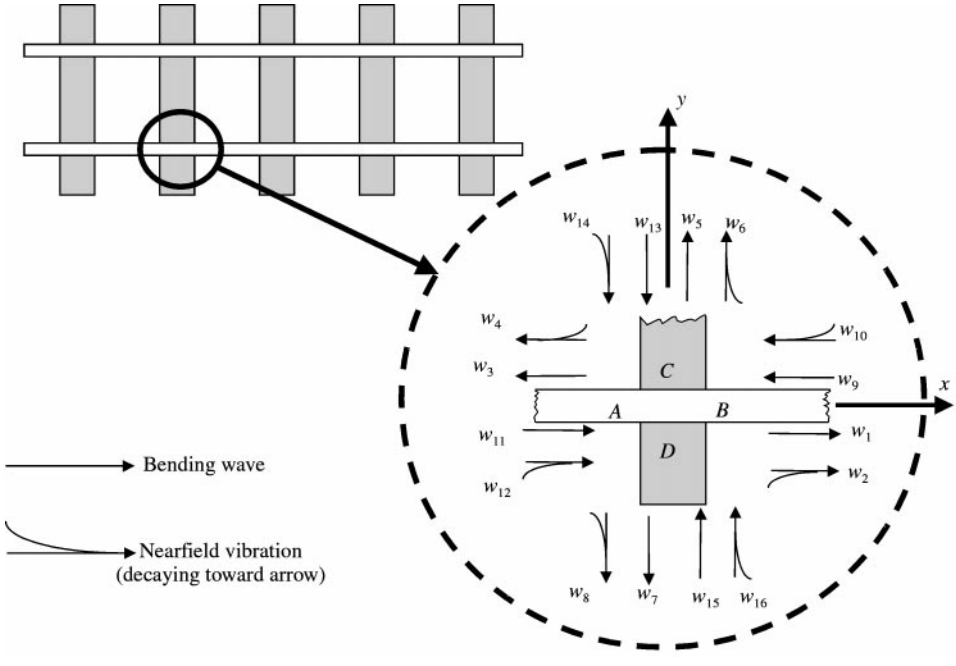

Figure 2. Waves and near fields at junction. Breakdown of displacements in z direction at points *A*, *B*, *C*, *D* into waves and near fields (with amplitudes in **w**). Odd (even) subscripts: bending waves (near fields).

$$z_B = (w_1 e^{-ik_{rB}x} + w_2 e^{-k_{rN}x} + w_9 e^{ik_{rB}x} + w_{10} e^{k_{rN}x}) e^{i\omega t}, \tag{2}$$

$$z_C = (w_5 e^{-ik_{SB}y} + w_6 e^{-k_{SN}y} + w_{13} e^{ik_{SB}y} + w_{14} e^{k_{SN}y}) e^{i\omega t}, \tag{3}$$

and

$$z_D = (w_7 e^{ik_{SB}y} + w_8 e^{k_{SN}y} + w_{15} e^{-ik_{SB}y} + w_{16} e^{-k_{SN}y}) e^{i\omega t}, \tag{4}$$

in which use is made of $k_{rB} \equiv k_{r1}$, $k_{rN} \equiv -ik_{r2}$, $k_{SB} \equiv k_{S1}$, and $k_{SN} \equiv -ik_{S2}$ where k_{r1}, k_{r2}, k_{S1}, and k_{S2} are the Timoshenko-theory bending wavenumbers for the rail (subscript r) and sleeper (subscript S), which are solutions to [14]

$$\frac{B_r^*}{M_r} k_r^4 - \frac{\omega^2}{A_r}\left(I_r + \frac{B_r^*}{G_r \tau_r}\right) k_r^2 - \omega^2 + \frac{M_r I_r}{G_r A_r^2 \tau_r} \omega^4 = 0 \tag{5}$$

and

$$\frac{B_S^*}{M_S} k_S^4 - \frac{\omega^2}{A_S}\left(I_s + \frac{B_S^*}{G_S \tau_S}\right) k_S^2 - \omega^2 + \frac{M_S I_S}{G_S A_S^2 \tau_S} \omega^4 + \frac{K_S}{M_S} + i\omega \frac{C_S}{M_S} = 0, \tag{6}$$

selecting subscripts 1 and 2 such that $k_{r1} \approx \mathrm{Re}(k_{r1}) > 0$, $k_{r2} \approx \mathrm{Im}(k_{r2}) < 0$, $k_{S1} \approx \mathrm{Re}(k_{S1}) > 0$, and $k_{S2} \approx \mathrm{Im}(k_{S2}) < 0$ (the $\approx$ due to losses). The frequency is assumed to be low enough such that the Timoshenko theory only gives one propagating solution (for each of the rail and the sleeper).

The Timoshenko-theory slope θ_A, bending moment M_A, and shear force F_A are related at A to the displacement z_A by (writing in such a form that the Euler–Bernoulli theory is recovered by keeping only the first terms on the right-hand sides):

$$\theta_A = \frac{\partial z_A}{\partial x} + \frac{1}{G_r A_r \tau_r}\left(B_r \frac{\partial^2 \theta_A}{\partial x^2} + M_r \omega^2 \theta_A\right), \tag{7}$$

$$M_A = B_r \frac{d\theta_A}{dx} \qquad F_A = -\frac{dM_A}{dx} - M_r \omega^2 \theta_A. \tag{8, 9}$$

For points B, C, and D, simply replace the subscript A; for C and D, subscript S replaces r.

The four components of the displacement (at any approach A, B, C, or D) may be interpreted physically as two bending waves and two near fields (see Figure 2). Thus, the figure introduces the symbols of straight arrows for bending waves and arrows with a "decaying curve" for near fields. The arrowhead indicates the direction of the bending wave propagation or of the nearfield decay. The subscripts for the elements of **w** may seem oddly selected, but are, nevertheless, systematic in a way which is convenient for later use: (i) odd subscripts are for bending wave amplitudes, and even for nearfield vibrations; (ii) subscripts $\leqslant 8$ indicate either a wave *incident* on the junction, or a near field which decays in a direction *approaching* the junction; a subscript > 8 indicates a wave *departing from* (i.e., transmitted or reflected) the junction or a near field decaying *away from* the junction; (iii) within each group of eight the first four subscripts pertain to the rail, and the last four to the sleeper.

2.3. JUNCTION CONDITIONS

Eight continuity and equilibrium conditions apply at a junction, and are collectively designated "junction conditions":

Continuity of rail displacement across junction:

$$z_A = z_B. \tag{10}$$

Continuity of sleeper displacement across junction:

$$z_C = z_D. \tag{11}$$

Continuity of rail slope across junction:

$$\theta_A = \theta_B. \tag{12}$$

Continuity of sleeper slope across junction:

$$\theta_C = \theta_D. \tag{13}$$

Equilibrium of rail moments across junction:

$$M_A = M_B. \tag{14}$$

Equilibrium of sleeper moments across junction:

$$M_C = M_D. \tag{15}$$

Equilibrium of rail shear force across junction:

$$K_Z^*[z_A - z_C] = F_A - F_B. \tag{16}$$

Equilibrium of sleeper shear force across junction:

$$K_Z^*[z_A - z_C] = F_C - F_D, \tag{17}$$

where F, M, θ and z are functions of $\mathbf{w}$ as indicated in equations (1)–(4), (7)–(9). These equations are repeated explicitly in terms of the amplitudes w in Appendix A.

2.4. JUNCTION INTERACTION WITH THE TRACK

2.4.1. *Connection of junction to free end of sleeper*

The sleeper has a free end at a distance y_0 from D. Thus, amplitudes w_{15} and w_{16} represent reflection of w_7 and w_8 there, with free-end boundary conditions, as well as decay and phase shift due to the double traverse of the distance y_0 along the sleeper:

$$w_{15} = \varepsilon_{BB} w_7 + \varepsilon_{NB} w_8, \qquad w_{16} = \varepsilon_{BN} w_7 + \varepsilon_{NN} w_8, \tag{18, 19}$$

where the complex "propagation-reflection" factors are (B is the bending wave, N the near field):

$$\varepsilon_{NN} = \mathrm{i}\mathrm{e}^{-2k_{SN}y_0}, \qquad \varepsilon_{NB} = (1+\mathrm{i})\,\mathrm{e}^{-(\mathrm{i}k_{SB}+k_{SN})y_0}, \tag{20, 21}$$

$$\varepsilon_{BN} = (1-\mathrm{i})\,\mathrm{e}^{-(\mathrm{i}k_{SB}+k_{SN})y_0}, \qquad \varepsilon_{BB} = -\mathrm{i}\mathrm{e}^{-2\mathrm{i}k_{SB}y_0}. \tag{22, 23}$$

2.4.2. *Connection of junction to the opposite side of the track*

Next, the influence of the second rail may be incorporated. Consider a second rail–sleeper junction across the track from the junction we have considered until now. This is located at $y = L_s - 2y_0$, referring to the geometry defined in section 2.1. This second junction (call it the "mirror junction"), has a 16-element vector of wave amplitudes analogous to $\mathbf{w}$ of the first junction; call this $\mathbf{w}'$. Furthermore, let $\mathbf{w}'$ be defined according to the "mirror" principle: such that w'_j has the same direction as w_j, for $j = 1, \ldots, 4, 9, \ldots, 12$ (i.e., waves/near fields on the rail), while w'_j has the opposite direction to w_j, for $j = 5, \ldots, 8, 13, \ldots, 16$ (i.e., waves/near fields on the sleeper). Using this definition, one may then write an "assembly condition" joining the two halves of the track together:

$$w'_{13} = w_5\mathrm{e}^{-\mathrm{i}k_s(L_s-2y_0)}, \qquad w'_{14} = w_6\mathrm{e}^{-k_s(L_s-2y_0)}, \tag{24, 25}$$

where the exponential terms represent decay and phase shift due to propagation across the track (from $y = 0$ to $L_s - 2y_0$).

The presumed excitation source of the track is the wheelset. It acts on both rails simultaneously, and its motion may be some combination of vertical and rolling rigid-body motions, as well as symmetric and antisymmetric bending mode shapes. Additionally, the track structure is symmetric with respect to its centreline. Thus, track modes will be excited in which the two rails vibrate with the same magnitude, but are possibly phase shifted. Thus,

$$w_{13} = \phi w'_{13}, \qquad w_{14} = \phi w'_{14}, \tag{26, 27}$$

where ϕ is a complex constant satisfying $|\phi| = 1$, which gives a phase shift φ between the rails, where $\phi = \mathrm{e}^{\mathrm{i}\varphi}$. Other motions, such as apparent independent vibration of a single rail, may be treated as summations of independent track modes.

Combining equations (25–28) gives

$$w_{13} = \zeta_B w_5, \qquad w_{14} = \zeta_N w_6, \tag{28, 29}$$

where we use the complex "propagation constants"

$$\zeta_B = \phi\mathrm{e}^{-\mathrm{i}k_s(L_s-2y_0)}, \qquad \zeta_N = \phi\mathrm{e}^{-k_s(L_s-2y_0)}. \tag{30, 31}$$

One may simply regard w_5 and w_6 as propagating away into an infinite sleeper, while w_{13} and w_{14} are contributed by a vibration source on the sleeper at $y = L_s - 2y_0$ (i.e., below the second rail). Observe that w_{13} and w_{14} *do not* represent reflections of w_5 and w_6. Instead, they are from a *source* which is identical to the considered junction (except for the phase shift φ).

The arbitrary complex constant ϕ can be regarded as representing the "*track mode*" (e.g., if the two rails are vibrating in antiphase, this is $\phi = -1$; if in phase, $\phi = +1$). Other values of ϕ are possible as well, and may be appropriate in practice. In fact, the track mode is determined by the excitation mechanism at the wheel, which is outside the subject area of this paper. For rolling noise, for instance, roughness on the two rails is likely to be

uncorrelated, so that both symmetric and antisymmetric modes are excited. Since they do not decay with the same attenuation however, one will dominate further along the track, and the net decay will not actually be exponential. For parametric excitation at the sleeper passing frequency, due to the periodic stiffness variation of the track (from the discrete support provided by the sleepers) [15], a symmetric track mode will be excited. A wheel flat on one wheel, as a third example, would give an equal combination of symmetric and antisymmetric excitation.

2.4.3. *Connection of junction to adjacent junctions on the rail*

A second subscript is applied to the elements of vector **w**, and which indicates the junction (numbered along the track, increasing in the positive x direction) at which **w** is evaluated. The Floquet assumption is now made that the decay along the track is exponential: $w_{p,j+1} = \mathrm{e}^{-a}\mathrm{e}^{-\mathrm{i}b} w_{p,j}$. Thus, noting that outgoing waves/near fields at junctions $j+1$ and $j-1$ propagate to junction j (e.g., w_3 at $j+1$ propagates leftwards to j, where it enters as w_9, etc.):

$$w_{9,j} = \gamma_B w_{3,j+1} = \mathrm{e}^{-a}\mathrm{e}^{-\mathrm{i}b}\gamma_B w_{3,j}, \qquad w_{10,j} = \gamma_N w_{4,j+1} = \mathrm{e}^{-a}\mathrm{e}^{-\mathrm{i}b}\gamma_N w_{4,j}, \quad (32, 33)$$

$$w_{11,j} = \gamma_B w_{1,j-1} = \mathrm{e}^{a}\mathrm{e}^{\mathrm{i}b}\gamma_B w_{1,j}, \qquad w_{12,j} = \gamma_N w_{2,j-1} = \mathrm{e}^{a}\mathrm{e}^{\mathrm{i}b}\gamma_N w_{2,j}, \quad (34, 35)$$

where $\gamma_B = \mathrm{e}^{-\mathrm{i}k_{rB}L}$ and $\gamma_N = \mathrm{e}^{-k_{rN}L}$ represent the decay and phase shift of a wave (or nearfield vibration) across the distance L between two adjacent junctions.

2.5. SOLUTION METHODOLOGY

Equations (A1)–(A8), (18), (19), (28), (29) and (32)–(35) provide a homogenous (16×16) matrix equation which is satisfied for particular values of $g \equiv a + \mathrm{i}b$. The lowest such positive value of a is the far field attenuation constant (per sleeper). A larger value of a gives decay in the source near field. Although the attenuation *per sleeper* is calculated directly, all results are presented as attenuation *per metre*.

3. RESULTS

All results, except as indicated, are for a typical Swedish light track on UIC-50 rails, referred to as the "reference track", and for which parameters are provided in Appendix B.

3.1. ASYMPTOTIC BEHAVIOUR

Asymptotic behaviour, at the limit of very stiff or very compliant support of the rail, is of interest because simple solutions for ideal cases are available to provide a verification of the wave method.

Figure 3 shows that the wave method result approaches the periodically pinned beam result (as in reference [16]) when the pad and foundation are made very stiff. Since the solution in reference [16] is for a Euler–Bernoulli beam, the Euler–Bernoulli models were also used in the wave method.

As the pads, on the other hand, become very soft, the attenuation approaches that of a free infinite beam with decay due to material losses only: $a \to -\mathrm{Im}(k_{rB})$, see Figure 4. At

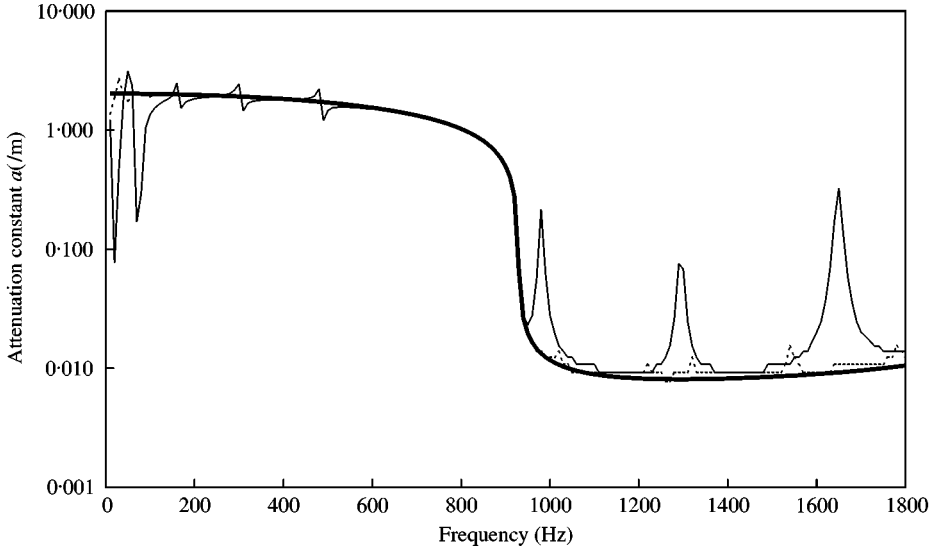

Figure 3. Asymptotic behaviour of the wave method for a firm foundation. ——, wave method (Euler–Bernoulli rail and sleeper) with $K_Z = 1 \times 10^{12}$ N/m, $M_S = 1 \times 10^4$ kg/m; ——, periodic pinned beam (period L and bending stiffness B_r) solution by method of [16]; – – – – –, wave method (Euler–Bernoulli rail and sleeper) with $K_Z = 1 \times 10^{12}$ N/m, $M_S = 1 \times 10^6$ kg/m.

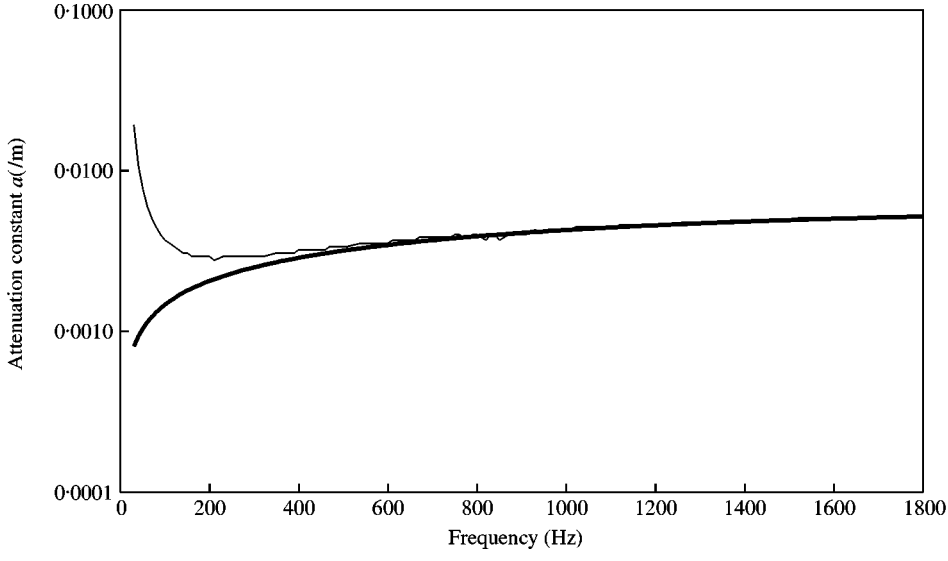

Figure 4. Asymptotic behaviour of the wave method for soft pads. ——, wave method with $K_Z = 5 \times 10^5$ N/m; ——, decay by hysteresis losses only in a Timoshenko beam with bending stiffness B_r and loss factor η.

the lowest frequencies, for which the pad (as a "spring") has high impedance (i.e., $K_z/i\omega$ is large), the deviation is still significant for the pad stiffness used. For a reduction of two more orders of magnitude, however, the two curves become indistinguishable above 10 Hz (not shown).

3.2. COMPARISON TO NUMERICAL RESULTS

For purposes of comparison, with more typical track component stiffnesses, a finite difference model of a finite track is used; this numerical model is detailed in reference [17]. It is based on the same physical model of the track, for the special case of Euler–Bernoulli models of the rail and sleeper, so that the comparison only provides a verification of the formulation, not the physical assumptions. The finite difference method is rather computationally intensive. Certainly, there are more sophisticated and efficient numerical methods than this one, but, since its use is limited to providing a one-time verification of the reasonableness of the wave propagation results, it is adequate. Figure 5 shows the predicted attenuation for the track detailed in Appendix B, with symmetric track mode, using both the wave method and the finite difference method (50-sleeper track). The same behaviour is predicted by both methods, but the finite difference method gives a higher attenuation below about 400 Hz (although the shape of the curves is the same). One calculation is carried out at 250 Hz, however, in which there are 100 sleepers. This result is in good agreement with the wave method. This suggests that the deviation between the two curves is due to the finite length of the track in the finite difference method, which, at low frequencies is too short.

3.3. COMPARISON TO FIELD MEASUREMENTS

Figure 6 compares the wave method predictions with measured results from a "Banklass 1" track near Söderhamn, Sweden. Such a track consists of UIC-60 rail and heavy concrete sleepers in stone ballast.

A single 11-g accelerometer was mounted to the rail foot (oriented vertically by use of an angle block). A hammer with a force transducer was then used to strike the rail head at two excitation points separated by a distance corresponding to four sleeper bays. Attenuation was determined from the difference in frequency response amplitude between the two excitation points. The measurement point and the hammer blows were on only one rail, so

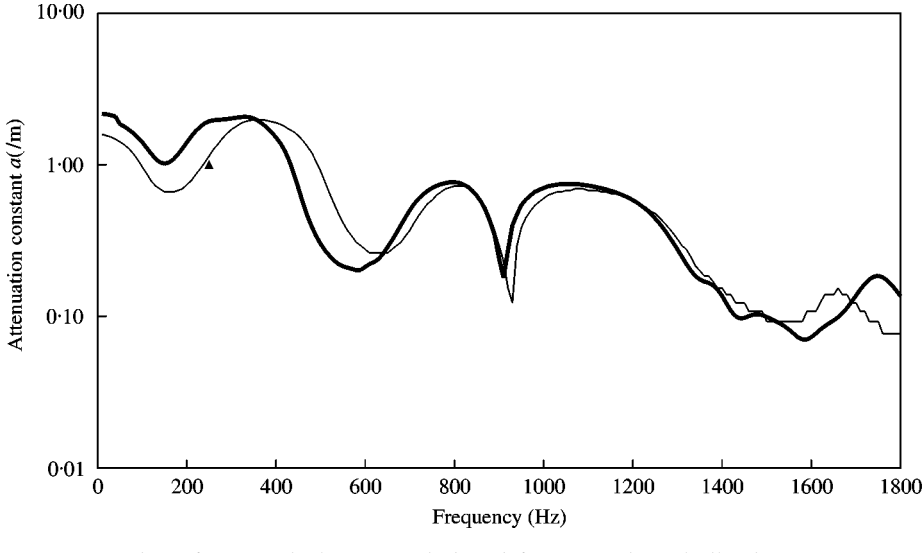

Figure 5. Comparison of wave method to a numerical result for symmetric track vibrations. ——, wave method (Euler–Bernoulli special case) with $B_r = 3\,244\,500$ N m^2; ——, finite difference method with $B_r = 3\,24\,4\,500$ N m^2, 50-sleeper track; ▲, finite difference method with $B_r = 3\,244\,500$ N m^2, 100-sleeper track.

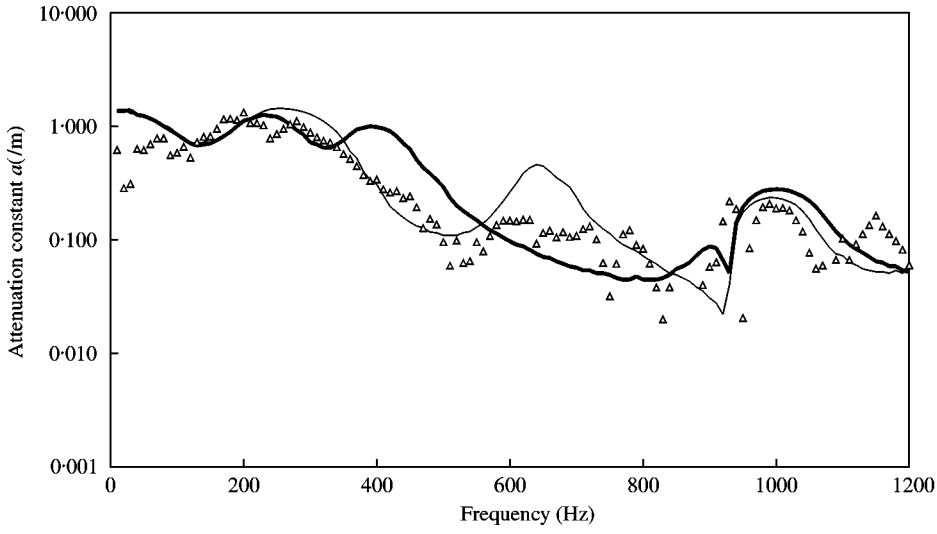

Figure 6. Comparison of wave method to field measurements. ——, wave method for UIC-60 track, symmetric vibration; ——, wave method for UIC-60 track, antisymmetric vibration; △, measured results from Swedish Banklass 1 track.

that, unfortunately, it is not possible to reconstruct the relative amplitudes of symmetric vibration and antisymmetric vibration (at the time the measurements were made, their use in the present context was not anticipated). The track, measurement conditions, and measurement technique are more fully detailed in reference [18].

The predicted results are based on typical track component parameter values for Banklass 1 track, since site-specific data were not available. The values differing from those of the reference track are [19]: $B_r = 4{\cdot}8 \times 10^6$ N m^2, $K_Z = 200$ MN/m, $M_r = 60{\cdot}3$ kg/m, $A_r = 7{\cdot}686 \times 10^{-3}$ m^2, $I_r = 30{\cdot}55 \times 10^{-6}$ m^4.

The comparison indicates that the prediction was acceptable up to 1200 Hz, but most especially at low frequencies. At high frequencies the attenuation is low, so that the measured amplitude differences between the two transducers are small. This makes the measured decay sensitive to noise. Accordingly, considerable scatter is observed.

It is also noted that, although both symmetric and antisymmetric vibrations should have been excited by the hammer blows, the experimental data most often follows the curve which indicates a lower attenuation. A plausible interpretation is that the more highly attenuated mode decays so much before reaching the transducer that the weakly attenuated mode dominates there (for blows at both excitation points).

3.4. EVALUATION OF SOME ASPECTS OF THE PHYSICAL MODEL

Predictions of attenuation in the reference track will now be used to illuminate the significance of some aspects of the physical model: track mode, choice of beam theory, and discreteness of the sleepers.

Attenuation predictions for both symmetric and antisymmetric vibrations are presented in Figure 7. As was even the case in Figure 3, the attenuation is high at low frequencies and low at high frequencies, with the transition occurring at about 860 Hz (at 930 Hz in Figure 3, because of the Euler–Bernoulli model there). This is the frequency at which a simply

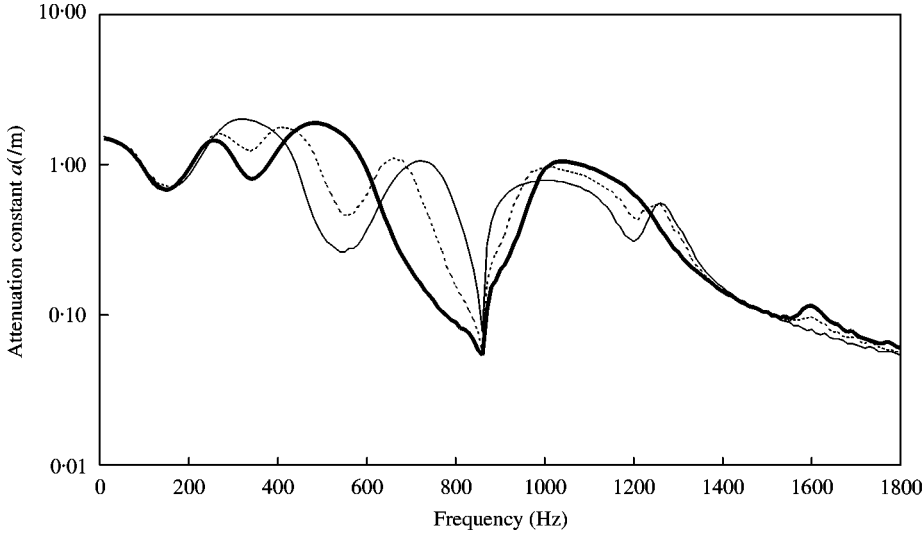

Figure 7. Attenuation prediction for Swedish light track. ——, symmetric track mode; ——, antisymmetric track mode; – – – – – –, vibrations with remote rail detached.

supported finite beam of length equal to the sleeper spacing L, and bending stiffness B_r, would have its first mode (the so-called "pinned–pinned" frequency).

With the more complicated model represented by Figure 7, however, more complicated behaviour is also predicted. Such behaviour can be attributed to the dynamic behaviour of the track components under the rail: the pads, sleepers, and ballast (which are ignored by the periodic pinned beam solution). There are three symmetric (at 127, 579 and 1230 Hz) and three antisymmetric (at 327, 880 and 1595 Hz) sleeper bending resonances in the considered frequency band. There is also a rigid-body resonance of the rail mass on the pad at about 612 Hz ("pad resonance"), and of the sleeper-plus-rail mass on the ballast at about 104 Hz ("ballast resonance"). The ballast resonance and the first (symmetric) sleeper bending resonance are so close together, that, with the damping provided by the ballast, their respective influences on the attenuation are indistinguishable.

Attenuation minima for symmetric vibrations occur at frequencies corresponding to symmetric sleeper resonances. For antisymmetric vibrations, these occur at antisymmetric sleeper resonances. These minima become less pronounced and eventually insignificant as the frequency becomes very high. Moreover, both symmetric and antisymmetric vibrations have an attenuation minimum at the ballast resonance. The first symmetric sleeper resonance, at nearly the same frequency, must have an insignificant effect in comparison, since both track modes have an attenuation minimum of about the same magnitude. The breadth of the second attenuation minimum, for the symmetric vibration, is also partly due to the pad resonance.

The difference in attenuation between the symmetric and antisymmetric cases can be significant at some frequencies. Near 700 Hz, for example, the figure predicts a difference in the attenuation constant of about 0·8/m, which corresponds to 7 dB/m additional attenuation (for the symmetric case, compared to the antisymmetric). The effect of track mode requires the incorporation of two rails into the model, as in the wave method. Figure 8 confirms that the wave propagation model agrees with the results of reference [7] when the second rail is detached (by replacing equations (15) and (16), in which the second rail acts as a source, with equations for a free reflection of w_5 and w_6 at the far end of the

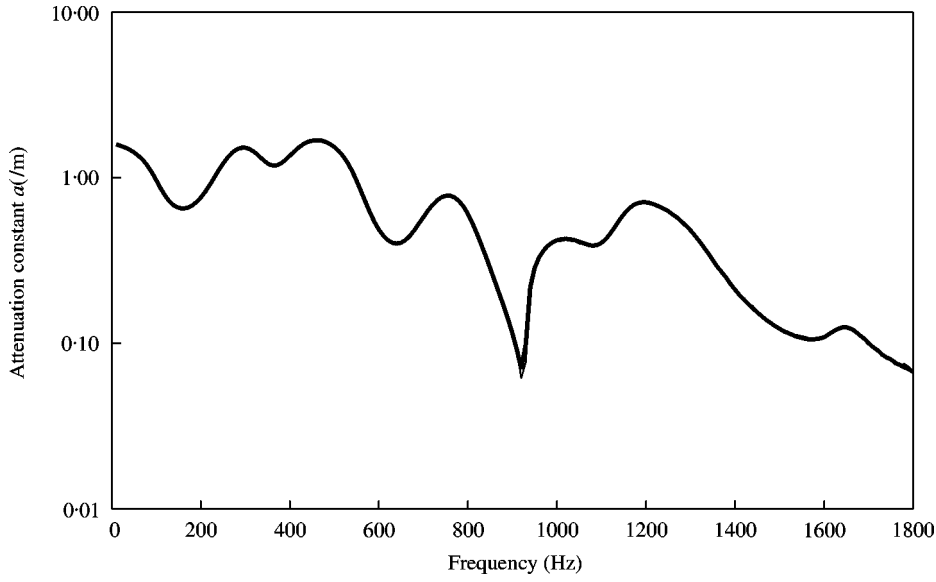

Figure 8. Attenuation in a track with the remote rail detached. ——, wave method (Euler–Bernoulli) with mirror source replaced by a simple reflection at the far end of the sleeper; ——, method of reference [7], with identical physical parameters.

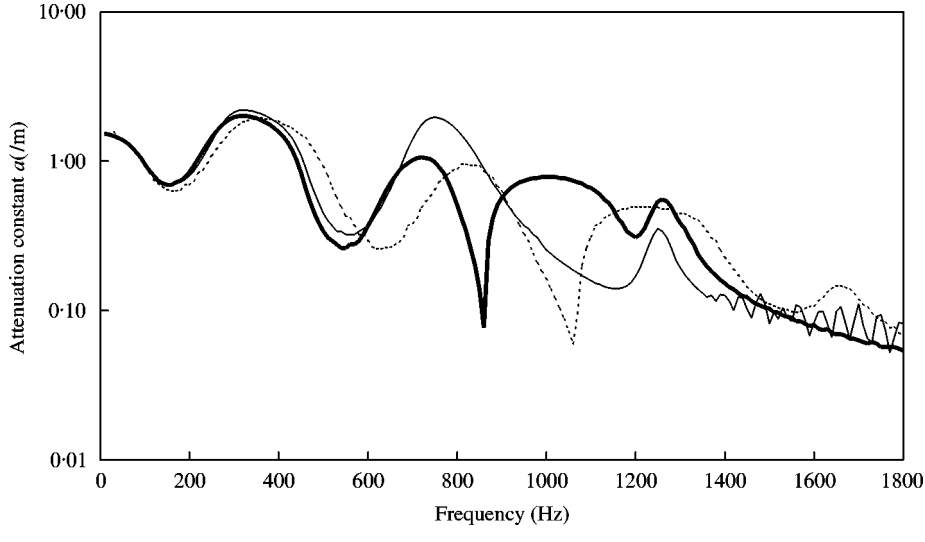

Figure 9. Attenuation predictions with variations of the physical model. ——, "continuous" track, Timoshenko models (wave method with $L = 0{\cdot}065$ m, and values of K_Z, B_S, I_S, A_S, M_S, K_S, C_S reduced by one order of magnitude with respect to the reference track); ——, discrete track, Timoshenko models; – – – – –, discrete track, Euler–Bernoulli models.

sleeper). Providing such a case in Figure 7, also, it is evident that a model incorporating only one rail will sometimes overpredict attenuation, and by extension, underpredict the radiated noise.

The effect of the discreteness of the sleepers can be seen in Figure 9, which compares a continuous track to the discrete one; the continuous track would correspond to the

physical model of reference [6]. The "continuous" track here is actually modelled by allowing L to become very small, while holding ratios K_z/L, B_S/L, I_S/L, A_S/L, M_S/L, K_S/L, and C_S/L constant. The main differences are near the pinned–pinned frequency, and in the band immediately above that.

Figure 9 also provides a comparison of the Timoshenko and the Euler–Bernoulli models. The location of the pinned–pinned frequency is the main difference.

3.5. PARAMETRIC STUDY

Figures 10–13 provide results of a small parametric survey, by comparing the reference track (the same as in Figure 4) with a track in which some design parameter is altered. The design parameter altered is pad stiffness (Figures 10 and 11), sleeper spacing (Figure 12), or sleeper length (Figure 13). All results are for symmetric track mode. Evidently, all of these parameters have a strong influence on the attenuation.

Increasing the pad stiffness (Figure 10) is seen to increase considerably the attenuation at high frequencies, above the pinned–pinned frequency. At low frequencies, there is a more modest attenuation increase, since the pad has a high impedance ($\propto \omega^{-1}$) in any case. A stiffer pad more firmly attaches the rail to the track below, and leads much energy down into the sleepers and ballast, where the losses are high. There is also increased dissipation in the pad itself. This echoes the results of reference [3] to the effect that a stiffer pad reduces the rail's "effective radiating length" (and, in consequence, the wayside noise); "effective radiating length" is used in reference [3] as a measure of attenuation, such that the smaller it is, the greater is the attenuation. It should be realized, however, that indefinitely increasing the pad stiffness will not continually give corresponding increases in attenuation. Figure 11 shows that the attenuation tends to a limit, so that the rail may at some point be regarded as "pinned" to the sleeper.

The pinned–pinned frequency itself, as can be seen, is independent of the pad stiffness. It is a function of the sleeper spacing L and of the rail bending stiffness B_r.

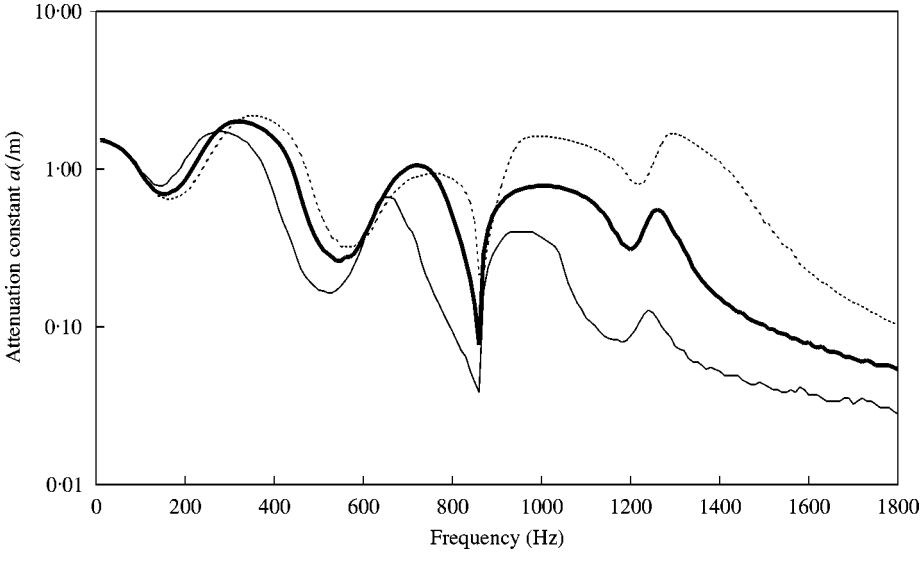

Figure 10. Effect of pad stiffness on attenuation. ——, $K_Z = 250$ MN/m; ——, $K_Z = 500$ MN/m (reference track); – – – – –, $K_Z = 1000$ MN/m.

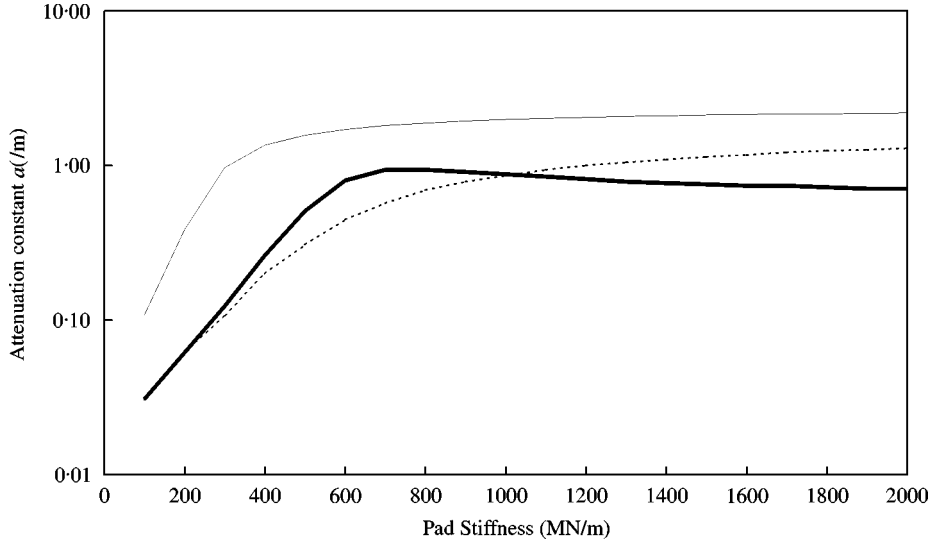

Figure 11. Effect of pad stiffness of attenuation. ——, 400 Hz; ——, 800 Hz; – – – – – –, 1200 Hz.

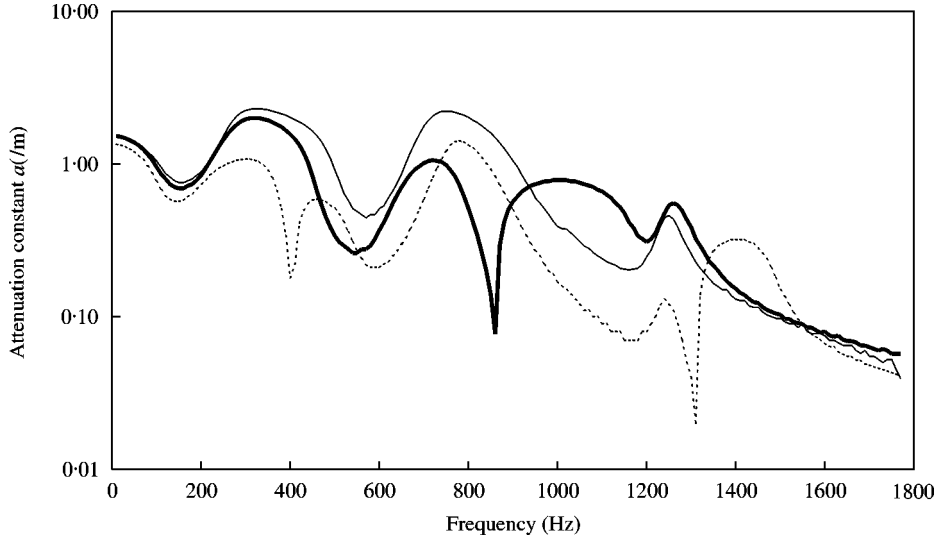

Figure 12. Effect of sleeper spacing on attenuation. ——, $L = 0{\cdot}4$ m; ——, $L = 0{\cdot}65$ m (reference track); – – – – –, $L = 1$ m.

The sleeper spacing effects the attenuation curves because it shifts the pinned–pinned frequency, whereas the various minima and maxima explainable by sleeper resonances and antiresonances remain unchanged. For the track considered, a change of the sleeper spacing *in either direction*, away from $L = 0{\cdot}65$ m, increases the attenuation around 860 Hz, by shifting away the pinned–pinned resonance. The pinned–pinned frequency is clearly seen at 400 Hz for the case $L = 1$ m, as is the second pinned–pinned frequency at 1310 Hz. For the case $L = 0{\cdot}4$ m, it is shifted to just outside of the plot (to 1840 Hz). It is also clear from the figure that, *in a broadband sense*, attenuation tends to decrease with increasing sleeper

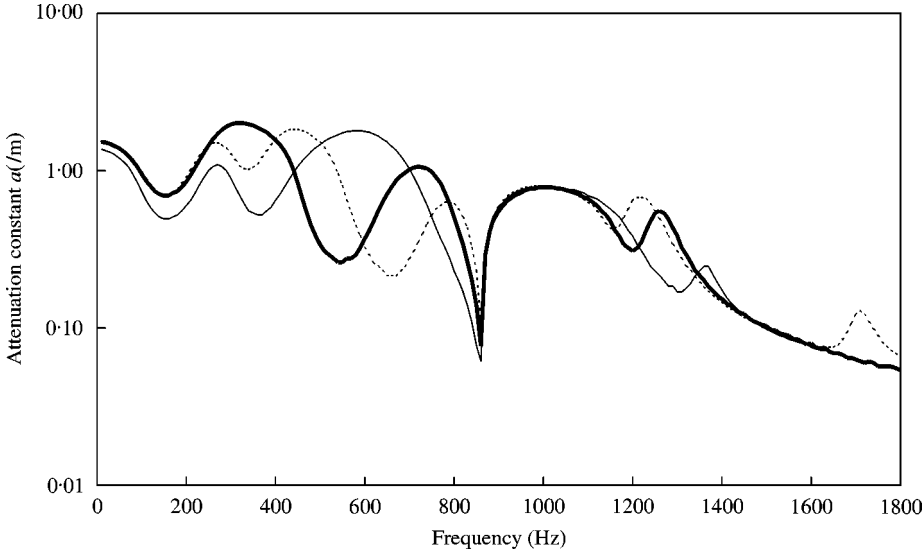

Figure 13. Effect of sleeper length on attenuation. ——, $L_S = 1{\cdot}5$ m (no overhang); ——, $L_S = 2{\cdot}5$ m (reference track); – – – – – –, $L_S = 3{\cdot}5$ m.

spacing. There are fewer reflecting–transmitting obstacles (i.e., the sleeper–rail junctions) over a given distance of track if the sleeper spacing is greater.

Moreover, the ballast resonance slightly decreases as L increases (observe the slight downward shift in the frequency of the first attenuation minimum with increasing sleeper spacing). While the stiffness under a single sleeper is constant, there is an increase in the length of rail supported above each sleeper. This effect is only slight, since the sleeper mass is much greater than the supported section of the rail in any case.

One also expects a decrease in the pad resonance with increasing L, again due to the increase in rail mass above each pad. Since the sleeper mass is not involved, the change should be greater than for the ballast resonance. Indeed, this is borne out by the considerable frequency shift of the second attenuation minimum when going from $L = 0{\cdot}4$ to 0·65 m. Nevertheless, it does not occur for the further increase to $L = 1$ m (in fact, there is a shift in the opposite direction).

For the sleeper length, Figure 13, the pinned–pinned frequency is unaffected (since it is only a function of the sleeper spacing), but the sleeper resonances and antiresonances shift, and thus also the various minima and maxima attributable to them.

4. SUMMARY AND CONCLUSIONS

Efficient predictions of attenuation in railway track are obtainable by a method based on the solution of wave (and near field) amplitudes at sleeper–rail junctions in an infinite track.

An important conclusion is that the attenuation is strongly dependent on the relative phase of vibration between the two rails, i.e., the "track mode". Antisymmetric vibration tends to have low attenuation bands at antisymmetric sleeper modes, while symmetric vibration has them, instead, at symmetric sleeper modes. A model lacking the second rail will, at some frequencies, overpredict the attenuation.

The attenuation depends also on track design, notably pad stiffness, sleeper spacing, and sleeper length.

ACKNOWLEDGMENTS

We express ous gratitude to the *Axel och Margaret Ax:son Johnson Stiftelse för Allmännyttiga Ändamål* for the funding of this work.

REFERENCES

1. D. J. THOMPSON 1988 *Journal of Sound and Vibration* **120**, 275–280. Predictions of acoustic radiation from vibrating wheels and rails.
2. Y. MORITOH, Y. ZENDA and K. NAGUKURA 1996 *Journal of Sound and Vibration* **193**, 319–334. Noise control of high speed Shinkansen.
3. N. VINCENT, P. BOUVET, D. J. THOMPSON and P. E. GAUTIER 1996 *Journal of Sound and Vibration* **193**, 161–171. Theoretical optimization of track components to reduce rolling noise.
4. J. C. O. NIELSEN 1993 *Ph.D. Thesis, Chalmers Tekniska Högskola, Göteborg, Sweden*. Train/Track Interaction: coupling of moving and stationary dynamic systems-theoretical and experimental analysis of railway structures considering wheel and track imperfections.
5. B. RIPKE 1994 *Ph.D. Thesis, Technische Universität, Berlin*. Hochfrequente gleismodellierung und simulation der fahrzeug-gleis-dynamik unter verwendung einer nichtlinearen kontaktmechanik. (Approximate translation: high frequency track modelling and simulation of vehicle–track dynamics by use of non-linear contact mechanics.)
6. S. L. GRASSIE and S. J. COX 1984 *Proceedings of IMechE* **198D**, 117–124. The dynamic response of a track with flexible sleepers to high frequency vertical excitation.
7. A. NORDBORG 1998 *Acustica* **84**, 280–288. Vertical rail vibrations: pointforce excitation.
8. M. A. HECKL 1992 *Report to the ORE (now ERRI) Committee C* 163, *Department of Mathematics, Keele University, Keele*. Coupled waves on a periodically supported Timoshenko beam.
9. S. L. GRASSIE, R. W. GREGORY, D. HARRISSON and K. L. JOHNSON 1982 *Journal Mechanical Engineering Science* **24**, 77–90. The dynamic response of railway track to high frequency vertical excitation.
10. M. L. MUNJAL and M. HECKL 1982 *Journal of Sound and Vibration* **81**, 491–500. Vibrations of a periodic rail–sleeper system excited by an oscillating stationary transverse force.
11. P. J. REMINGTON 1987 *Journal of Acoustical of the Society of America* **81**, 1805–1823. Wheel/rail rolling noise I: theoretical analysis.
12. D. J. THOMPSON and N. VINCENT 1995 *Vehicle System Dynamics Supplement* **24**, 86–99. Track dynamic behaviour at high frequencies. Part 1: theoretical models and laboratory measurements.
13. D. J. THOMPSON 1993 *Journal of Sound and Vibration* **161**, 421–446. Wheel–rail noise generation, Part III: rail vibration.
14. K. F. GRAFF 1975 *Wave Motion in Elastic Solids*. New York: Dover Publications.
15. A. NORDBORG 1998 Acustica **84**, 289–300. Vertical rail vibrations: parametric excitation.
16. L. CREMER, M. HECKL and E. E. UNGAR 1988 *Structure-Borne Sound: Structural Vibrations and Sound Radiation at Audio Frequencies*. Berlin: Springer, second edition.
17. R. HILDEBRAND 1999 *TRITA-FKT* 9915, *Department of Vehicle Engineering, KTH (Royal Institute of Technology), Stockholm*. Sound attenuation in railway track.
18. U. CARLSSON and R. HILDEBRAND 1999 *TRITA-FKT* 9955, *Department of Vehicle Engineering, KTH, Stockholm*. Spårprototyp i Norraladalen: utvärdering avseende ljud och vibrationer (translation: Track prototype in Norraladalen: vibroacoustic assessment).
19. E. ANDERSSON and M. BERG 1999 Järnvägssystem och spårfordon, del 1: Järnvägssystem. *Järnvägsgruppen, KTH, Stockholm* (translation: Railway systems and track vehicles).

APPENDIX A: JUNCTION EQUATIONS EXPLICITLY IN TERMS OF w

$$-w_1 - w_2 + w_3 + w_4 - w_9 - w_{10} + w_{11} + w_{12} = 0, \tag{A1}$$

$$w_5 + w_6 - w_7 - w_8 + w_{13} + w_{14} - w_{15} - w_{16} = 0, \tag{A2}$$

$$\begin{aligned} &\mathrm{i}(k_{rB} - \chi_{rB})w_1 + (k_{rN} - \chi_{rN})w_2 + \mathrm{i}(k_{rB} - \chi_{rB})w_3 + (k_{rN} - \chi_{rN})w_4 \\ &- \mathrm{i}(k_{rB} - \chi_{rB})w_9 - (k_{rN} - \chi_{rN})w_{10} - \mathrm{i}(k_{rB} - \chi_{rB})w_{11} - (k_{rN} - \chi_{rN})w_{12} = 0, \end{aligned} \tag{A3}$$

$$-\mathrm{i}(k_{SB}-\chi_{SB})w_5-(k_{SN}-\chi_{SN})w_6+\mathrm{i}(k_{SB}-\chi_{SB})w_7+(k_{SN}-\chi_{SN})w_8$$

$$+\mathrm{i}(k_{SB}-\chi_{SB})w_{13}+(k_{SN}-\chi_{SN})w_{14}+\mathrm{i}(k_{SB}-\chi_{SB})w_{15}+(k_{SN}-\chi_{SN})w_{16}=0, \tag{A4}$$

$$(k_{rB}^2-k_{rB}\chi_{rB})w_1-(k_{rN}^2-k_{rN}\chi_{rN})w_2-(k_{rB}^2-k_{rB}\chi_{rB})w_3+(k_{rN}^2-k_{rN}\chi_{rN})w_4$$

$$+(k_{rB}^2-k_{rB}\chi_{rB})w_9-(k_{rN}^2-k_{rN}\chi_{rN})w_{10}-(k_{rB}^2-k_{rB}\chi_{rB})w_{11}+(k_{rN}^2-k_{rN}\chi_{rN})w_{12}=0, \tag{A5}$$

$$-(k_{SB}^2-k_{SB}\chi_{SB})w_5+(k_{SN}^2-k_{SN}\chi_{SN})w_6+(k_{SB}^2-k_{SB}\chi_{SB})w_7-(k_{SN}^2-k_{SN}\chi_{SN})w_8$$

$$-(k_{SB}^2-k_{SB}\chi_{SB})w_{13}+(k_{SN}^2-k_{SN}\chi_{SN})w_{14}+(k_{SB}^2-k_{SB}\chi_{SB})w_{15}$$

$$-(k_{SN}^2-k_{SN}\chi_{SN})w_{16}=0, \tag{A6}$$

$$(\mathrm{i}(k_{rB}^3-k_{rB}^2\chi_{rB})-\Xi_{rB})w_1-(k_{rN}^3-k_{rN}^2\chi_{rN}+\Xi_{rN})w_2+\left(\frac{K_Z^*}{B_r^*}+\mathrm{i}(k_{rB}^3-k_{rB}^2\chi_{rB})-\Xi_{rB}\right)w_3$$

$$+\left(\frac{K_Z^*}{B_r^*}-(k_{rN}^3-k_{rN}^2\chi_{rN})-\Xi_{rN}\right)w_4-\frac{K_Z^*}{B_r^*}w_5-\frac{K_Z^*}{B_r^*}w_6-(\mathrm{i}(k_{rB}^3-k_{rB}^2\chi_{rB})-\Xi_{rB})w_9$$

$$+(k_{rN}^3-k_{rN}^2\chi_{rN}+\Xi_{rN})w_{10}+\left(\frac{K_Z^*}{B_r^*}-\mathrm{i}(k_{rB}^3-k_{rB}^2\chi_{rB})+\Xi_{rB}\right)w_{11}$$

$$+\left(\frac{K_Z^*}{B_r^*}+(k_{rN}^3-k_{rN}^2\chi_{rN})+\Xi_{rN}\right)w_{12}-\frac{K_Z^*}{B_r^*}w_{13}-\frac{K_Z^*}{B_r^*}w_{14}=0, \tag{A7}$$

$$\frac{K_Z^*}{B_S^*}w_3+\frac{K_Z^*}{B_S^*}w_4+\left(-\mathrm{i}(k_{SB}^3-k_{SB}^2\chi_{SB})+\Xi_{SB}-\frac{K_Z^*}{B_S^*}\right)w_5+\left((k_{SN}^3-k_{SN}^2\chi_{SN})+\Xi_{SN}-\frac{K_Z^*}{B_S^*}\right)w_6$$

$$+(\Xi_{SB}-\mathrm{i}(k_{SB}^3-k_{SB}^2\chi_{SB}))w_7+(k_{SN}^3-k_{SN}^2\chi_{SN}+\Xi_{SN})w_8+\frac{K_Z^*}{B_S^*}w_{11}+\frac{K_Z^*}{B_S^*}w_{12}$$

$$+\left(\mathrm{i}(k_{SB}^3-k_{SB}^2\chi_{SB})-\Xi_{SB}-\frac{K_Z^*}{B_S^*}\right)w_{13}+\left(-(k_{SN}^3-k_{SN}^2\chi_{SN})-\Xi_{SN}-\frac{K_Z^*}{B_S^*}\right)w_{14}$$

$$+(-\Xi_{SB}+\mathrm{i}(k_{SB}^3-k_{SB}^2\chi_{SB}))w_{15}+(-(k_{SN}^3-k_{SN}^2\chi_{SN})-\Xi_{SN})w_{16}=0. \tag{A8}$$

The junction conditions include the following terms which contain the entire Timoshenko correction: $\chi_{rB}=M_r\omega^2/k_{rB}G_rA_r\tau_r$, $\chi_{rN}=-M_r\omega^2/k_{rN}G_rA_r\tau_r$, $\chi_{SB}=M_S\omega^2/k_{SB}G_SA_S\tau_S$, $\chi_{SN}=-M_S\omega^2/k_{SN}G_SA_S\tau_S$, $\Xi_{rB}=M_rI_r\omega^2\mathrm{i}(k_{rB}-\chi_{rB})/B_r^*$, $\Xi_{rN}=M_rI_r\omega^2(k_{rN}-\chi_{rN})/B_r^*$, $\Xi_{SB}=M_SI_S\omega^2\mathrm{i}(k_{SB}-\chi_{SB})/B_S^*$, and $\Xi_{SN}=M_SI_S\omega^2(k_{SN}-\chi_{SN})/B_S^*$. For the special case of Euler–Bernoulli theory, it suffices to set these terms to zero, $\chi_{rB}=\chi_{rN}=\chi_{SB}=\chi_{SN}=\Xi_{rB}=\Xi_{rN}=\Xi_{SB}=\Xi_{SN}=0$, and to use $k_{rB}^4=k_{rN}^4=M_r\omega^2/B_r^*$ and $k_{sB}^4=k_{sN}^4=(M_S\omega^2-K_S-\mathrm{i}\omega C_S)/B_S^*$.

APPENDIX B: SYMBOLS AND REFERENCE VALUES FOR SAMPLE RESULTS

Values represent typical Swedish light track on UIC-50 rails ("reference track").

$A_r = 6{\cdot}75 \times 10^{-3}$ m^2	cross-sectional area of rail
$A_S = 3{\cdot}85 \times 10^{-2}$ m^2	cross-sectional area of sleeper
$B_S = 4{\cdot}6 \times 10^6$ N m^2	Euler–Bernoulli bending stiffness of sleeper (x-axis)
$B_r = 4\,294\,500$ N m^2	Euler–Bernoulli bending stiffness of rail (y-axis)
$C_S = 6 \times 10^4$ N s/m^2	damping per unit length (along sleeper) of ballast
$G_r = 7{\cdot}62 \times 10^{10}$ Pa	shear modulus of rail
$G_S = 1{\cdot}11 \times 10^{10}$ Pa	shear modulus of sleeper
$I_r = 15{\cdot}45 \times 10^{-6}$ m^4	moment of inertia of rail cross-section
$I_S = 1{\cdot}84 \times 10^{-4}$ m^4	moment of inertia of sleeper cross-section
$K_S = 6 \times 10^7$ N/m^2	stiffness per unit length (along sleeper) of ballast
$K_Z = 5 \times 10^8$ N/m	pad stiffness in normal deformation
$L = 0{\cdot}65$ m	sleeper spacing
$L_S = 2{\cdot}5$ m	sleeper length
$M_r = 52{\cdot}0$ kg/m	length density of rail
$M_S = 100$ kg/m	length density of sleeper
$y_0 = 0{\cdot}5$ m	sleeper overhang
$\eta = 0{\cdot}004$	rail loss factor
$\eta_S = 0{\cdot}01$	sleeper loss factor
$\eta_Z = 0{\cdot}15$	pad loss factor in normal deformation
$\tau_r = 0{\cdot}4$	Timoshenko constant for rail (as defined in reference [14])
$\tau_S = 0{\cdot}83$	Timoshenko constant for sleeper (as defined in reference [14])

The complex sleeper, rail, and pad stiffnesses (indicated by a superscripted *) are given by $B_S^* = B_S\,(1 + \mathrm{i}\eta_S)$, $B_r^* = B_r\,(1 + \mathrm{i}\eta)$, and $K_Z^* = K_Z\,(1 + \mathrm{i}\eta_Z)$ respectively.